Higher Order Spatial Operators for the Finite Integration Theory

Holger Spachmann, Rolf Schuhmann, Thomas Weiland
Technische Universität Darmstadt, FB 18, Theorie Elektromagnetischer Felder (TEMF),
Schlossgartenstr. 8, D-64289 Darmstadt, Germany
eMail: spachmann/schuhmann/weiland@temf.de

Abstract— **The Finite Integration Technique (*FIT*) according to T. Weiland [1] is an efficient and universal method for solving a large scale of problems in computational electrodynamics. Up to now the conventional formulation itself has had an accuracy order of two with respect to the spatial discretization. In this paper an innovative extension to fourth or even higher order is presented. The convergence of the presented scheme is demonstrated by a general dispersion equation and stability issues are discussed. An approach for a stable spatial interface connecting regions of higher order with the standard *FIT* scheme is proposed.**

Keywords— **Finite Integration Technique, FDTD, higher order modeling, numerical dispersion**

I. Introduction

During the last years a lot of approaches towards higher order spatial finite difference (*FD*) schemes have been developed. Improved spatial discretization is normally achieved by modification of the discrete curl operator resulting in wideranging spatial schemes for static [2], transient [3], [4] and frequency-domain [5] problems. Approaches using interpolating functions for fields with cubic splines were also developed [6].

In transient field analysis especially in the finite difference time domain scheme (*FDTD*) combined methods for explicit higher order spatial resolution and time integration are presented in [7]-[10]. These approaches use substitutions of higher order time derivatives by spatial derivatives leading to higher order Leap-Frog schemes or Runge-Kutta integration methods. Recent approaches mix higher order spatial and temporal differencing schemes to obtain a full fourth order accurate scheme for transient field simulation [12]. A completely different approach utilizes multi-resolution functions and wavelets for representation of fields leading to higher order formulations in space [13]. This approach is currently discussed and modified by various authors.

In this paper an efficient spatial formulation of arbitrary order for the Finite Integration Technique is presented and its applicability in the case of a fourth order scheme (*FIT*-4) is demonstrated.

As one of the key points in the theory of *FIT*, the modeling procedure of Maxwell's Equations can be separated into two steps. In the first step, the discretization of the equations themselves, the so called Maxwell's Grid Equations are derived. Based on the concept of grid voltages and grid fluxes they represent an *exact* transformation of the continuous relations to grid space, as the integrals used are only specialized to a finite set of integration paths (along edges of the grids) or integration volumes (cells of the grids), respectively.

Thus, the approximations of the method do not come into effect until the material matrices are introduced (the second modeling step). For the derivation of these discrete analogs of the continuous constitutive relations, the integral state variables (fluxes and voltages) have to be retransformed to actual field components, as will be explained in more detail later. For the conventional *FIT* [1], the transformation of flux into voltage quantities has typically a second order accuracy.

From this point of view, the path to an extension to higher order schemes has naturally to be the following. Rather than introducing higher order schemes for the differential operators curl and div (as in the *FD* literature [2]-[12]), or defining higher order basis functions for single cells (as in p-adaptive finite element schemes), utilizing an increased number of degrees of freedom per cell, "only" the material matrices have to be replaced by suitable higher order operators. As an important consequence, as long as some basic requirements for the new material matrices are met, all the well-known consistency and conservation properties of *FIT* [14] can be preserved.

II. Basic Concepts

A. FI-Technique

The formulation of the Finite Integration Technique proposed by T. Weiland [1], [15] provides a general spatial discretization scheme usable for different electromagnetic applications of arbitrary geometry, e.g. static and quasi-static problems or calculations in frequency- and time-domain.

The geometry is discretized on a dual-orthogonal grid set consisting of the primary grid G (with the edges Δl, the facets ΔA and the material distribution) and the so called dual grid $\tilde{G}$ (containing the dual edges $\Delta\tilde{l}$ and dual facets $\Delta\tilde{A}$). In contrast to the vectors of elementary

field values $\mathbf{e}$, $\mathbf{d}$, $\mathbf{h}$, $\mathbf{b}$, the *FIT* deals with the integral expressions

$$\widehat{e} = \int_{\Delta l} \vec{E} \cdot d\vec{s}, \tag{1a}$$

$$\widehat{h} = \int_{\Delta \tilde{l}} \vec{H} \cdot d\vec{s}, \tag{1b}$$

$$\widehat{\tilde{d}} = \int_{\Delta \tilde{A}} \vec{D} \cdot d\vec{A}, \tag{1c}$$

$$\widehat{\tilde{b}} = \int_{\Delta A} \vec{B} \cdot d\vec{A} \tag{1d}$$

which form the components of the vectors $\widehat{\mathbf{e}}$, $\widehat{\tilde{\mathbf{d}}}$, $\widehat{\mathbf{h}}$ and $\widehat{\tilde{\mathbf{b}}}$, being indicated by bows. The components of the vectors of electric voltage $\widehat{\mathbf{e}}$ and magnetic flux $\widehat{\tilde{\mathbf{b}}}$ are located on the primary grid G, and the components of the vectors of electric flux $\widehat{\tilde{\mathbf{d}}}$, electric current $\widehat{\tilde{\mathbf{j}}}$ and magnetic voltage $\widehat{\mathbf{h}}$ on the dual grid $\tilde{G}$ (see Fig. 1).

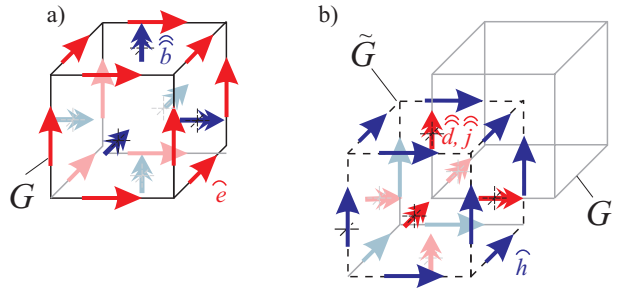

Fig. 1. Location of electric voltage $\widehat{e}$ on edges and magnetic flux $\widehat{\tilde{b}}$ on facets of primary grid G (a) and magnetic voltage $\widehat{h}$ on edges and electric flux $\widehat{\tilde{d}}$ and electric current $\widehat{\tilde{j}}$ on facets of dual grid $\tilde{G}$ (b).

The *FIT* formulation results in the so called Maxwell Grid Equations (*MGEs*)

$$\mathbf{C}\widehat{\mathbf{e}} = -\frac{d}{dt}\widehat{\tilde{\mathbf{b}}}, \tag{2a}$$

$$\widetilde{\mathbf{C}}\widehat{\mathbf{h}} = \frac{d}{dt}\widehat{\tilde{\mathbf{d}}} + \widehat{\tilde{\mathbf{j}}} + \widehat{\tilde{\mathbf{j}}}_{ext}, \tag{2b}$$

$$\widetilde{\mathbf{S}}\widehat{\tilde{\mathbf{d}}} = \mathbf{q}, \tag{2c}$$

$$\mathbf{S}\widehat{\tilde{\mathbf{b}}} = \mathbf{0}, \tag{2d}$$

whereby the curl matrices ($\mathbf{C}$, $\widetilde{\mathbf{C}}$) and the source matrices ($\mathbf{S}$, $\widetilde{\mathbf{S}}$) represent a summation scheme for the closed line integral around each cell facet and closed surface integral over each cell volume, thus providing the topological relation needed by Maxwell's integral equations applied to the grid set. The numerical character of the spatial operators [14] are vital for the underlying consistency of the conventional *FIT* formulation

$$\mathbf{SC} \equiv 0, \tag{3a}$$

$$\widetilde{\mathbf{S}}\widetilde{\mathbf{C}} \equiv 0, \tag{3b}$$

$$\mathbf{C} = \widetilde{\mathbf{C}}^T \tag{3c}$$

which reflect the properties of its analytical pendant.

For connecting the voltage and flux quantities, the constitutive relations

$$\widehat{\mathbf{e}} = \mathbf{M}_{\varepsilon^{-1}}\widehat{\tilde{\mathbf{d}}}, \tag{4a}$$

$$\widehat{\mathbf{h}} = \mathbf{M}_{\mu^{-1}}\widehat{\tilde{\mathbf{b}}}, \tag{4b}$$

$$\widehat{\mathbf{e}} = \mathbf{M}_{\kappa^{-1}}\widehat{\tilde{\mathbf{j}}} \tag{4c}$$

with the discrete material matrices $\mathbf{M}_{\varepsilon^{-1}}$, $\mathbf{M}_{\mu^{-1}}$ and $\mathbf{M}_{\kappa^{-1}}$ are introduced. They are responsible for the discretization errors of the method and thus are the key point of the derivations in the following sections.

III. Higher Order Material Relation

As explained before the *MGEs* deal only with the topological relation of the involved electric and magnetic quantities. Therefore the pure application of (2) is exact i.e. no discretization process is applied. The constitutive relations (4) connect fluxes through facets of one grid with voltages along edges of the corresponding dual grid which intersect these facets normally. The calculation of the coupling coefficients includes the metric of the grid as well as the material distribution.

The scheme connecting fluxes with voltages has to take into account the Maxwellian continuity law of the tangential field strength and normal flux density at material boundaries

$$E_{tan}(\vec{r}_-, t) = E_{tan}(\vec{r}_+, t), \tag{5a}$$

$$J_A(\vec{r}) = H_{tan}(\vec{r}_-, t) - H_{tan}(\vec{r}_+, t), \tag{5b}$$

$$B_{norm}(\vec{r}_-, t) = B_{norm}(\vec{r}_+, t), \tag{5c}$$

$$q_A(\vec{r}) = D_{norm}(\vec{r}_-, t) - D_{norm}(\vec{r}_+, t) \tag{5d}$$

with the surface current J_A and the surface charge q_A. These laws ensure in the case of surface charge and surface current free regions the continuity of the tangential field strength and normal flux density of the electric and magnetic field.

A. Conventional FIT Material Relation

In the following, a dual-orthogonal grid set with the general coordinates u, v and w is regarded. For simplicity reasons, the flux to voltage transformation is considered only for the magnetic field, the conversion mechanism for the electric field is straightforward. Conventional *FIT* calculates the coupling coefficients of magnetic flux to magnetic voltage in a two step process.

1. The flux density is derived from the flux through the related facet ΔA of the primary grid. The definition of the magnetic flux through a cell facet

$$\widehat{\widehat{b}} = \int_{\Delta A} \vec{B} \cdot d\vec{A}, \tag{6}$$

ends in conventional FIT in the approximation

$$\widehat{\widehat{b}} = b \cdot \Delta A + \mathcal{O}(\Delta l^4), \tag{7}$$

whereby the local flux density b is located at the center of the related facet.

2. The locally calculated flux density is converted to voltage by integrating it along the corresponding cell edge, resulting in the multiplication of the flux density value with a quotient of edge length and proper averaged material value respecting (5c)

$$\begin{aligned}\widehat{h} &= \int_{\Delta l_1/2} \mu_1^{-1}\vec{B} \cdot d\vec{s} + \int_{\Delta l_2/2} \mu_2^{-1}\vec{B} \cdot d\vec{s} \\ &= \mu_1^{-1} b \frac{\Delta l_1}{2} + \mu_2^{-1} b \frac{\Delta l_2}{2} + \mathcal{O}(\Delta l^{2\cdots 3}).\end{aligned} \tag{8}$$

The length of the dual cell edge is given by $\Delta\tilde{l} = \Delta l_1/2 + \Delta l_2/2$, Δl_1 and Δl_2 associated to the adjacent cells of the primary grid. A full third order scheme is guaranteed, if the grid is equally spaced and the materials homogeneous, otherwise the local conversion order decreases down to $\mathcal{O}(\Delta l^2)$.

This two step process ends in the following formula, describing the generalized material coefficients for the transformation of magnetic flux into magnetic voltage

$$\begin{aligned}\underbrace{\int_{\Delta\tilde{l}_n} \vec{H} \cdot d\vec{s}}_{\widehat{h}_n} &= \frac{\Delta\tilde{l}_n}{\bar{\mu}_{av.}\Delta A_n} \underbrace{\int_{\Delta\bar{A}_n} \vec{B} \cdot d\vec{A}}_{\widehat{\widehat{b}}_n} + \mathcal{O}(\Delta l^{2\cdots 3}) \\ &\approx M_{\mu}^{-1}{}_{n,n}\, \widehat{\widehat{b}}_n\end{aligned} \tag{9}$$

with

$$\frac{1}{\bar{\mu}_{av.}} = \frac{\frac{\Delta l_{n_1}}{\mu_1} + \frac{\Delta l_{n_2}}{\mu_2}}{\Delta\tilde{l}_n}. \tag{10}$$

The necessary metric information, material distribution and location of the flux and voltage values for the magnetic field is displayed in Fig.2, for the electric field in Fig. 3. The resulting material coefficients represent cell inductances, cell capacities and cell resistances, respectively.

B. Principles of Higher Order Spatial Discretization

The new higher order material modeling is a three step process utilizing piece-wise defined polynomials and following the basic ideas of the conventional FIT.

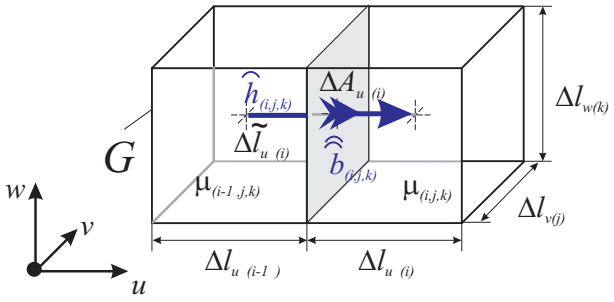

Fig. 2. Relation of magnetic flux $\widehat{\widehat{b}}$ with magnetic voltage $\widehat{h}$ in conventional FIT.

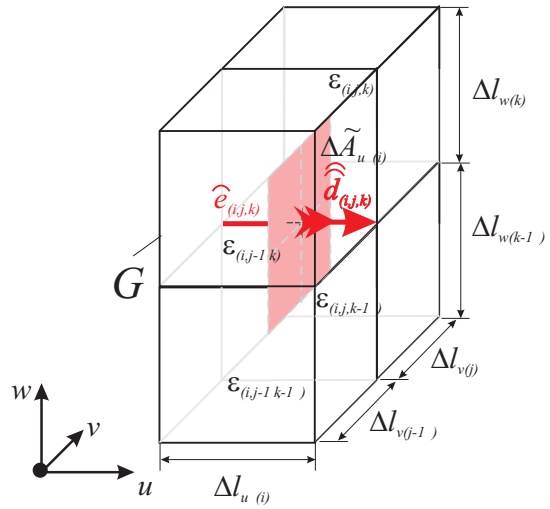

Fig. 3. Relation of electric flux $\widehat{\widehat{d}}$ with electric voltage $\widehat{e}$ in conventional FIT.

- *Approximation* of integrals associated to surfaces (flux) or edges (voltage) with a suitable localized higher order polynomial function describing field strength or flux density (in conventional FIT they are assumed to be constant along the edges).
- *Conversion* of the derived field strength- or flux density values locally in their equivalent flux density- or field strength values respectively.
- *Interpolation* of these field values by another localized higher order polynomial function enables the calculation of the desired voltages respectively fluxes.

Note that in contrast to other higher order approaches using wideranging spatial differential operators, this new approach leaves $\mathbf{C}$ and $\mathbf{S}$ untouched, thus the properties of FIT (3) [14] still hold for this discretization technique.

In the following section, a general method for deriving higher order conversion schemes for surface based (flux) in edge based (voltage) quantities is discussed and an exemplarily approach for fourth order modeling (FIT-4 scheme) is presented. Once again for simplicity reasons the discussion is restricted to the conversion scheme for the magnetic field, the construction of the scheme for the

electric quantities or the conductivity current is straightforward. As seen before for the conventional scheme, a local decrease of the convergence rate is inflicted by non-equidistant grid spacing or inhomogenious material distribution.

C. Higher Order Flux to Voltage Conversion

C.1 Derivation of Flux

The new approach assumes a piece-wise defined higher order magnetic field strength function $h(u,v)$ describing the normal field component on a surface consisting of facets $A_{(n,m)}$. The surface integral of the assumed function multiplied by a material weighting function $\mu(u,v)$ approximates the magnetic flux through the surface considering (5b) and assuming surface current free regions.

For example a localized biquadratic formulation of the normal field strength function on the facets $\Delta A_{w_{(i,j)}}$, $\Delta A_{w_{(i+1,j)}}$, $\Delta A_{w_{(i-1,j)}}$, $\Delta A_{w_{(i,j+1)}}$ and $\Delta A_{w_{(i,j-1)}}$ can be written as

$$h_w(u,v) = a_1 + a_2 \cdot u + a_3 \cdot v + a_4 \cdot u^2 + a_5 \cdot v^2 \quad (11)$$

with the five unknowns $a_1,\ a_2,\ \cdots, a_5$. Starting with the five flux values $\hat{\tilde{b}}_{w_{(i,j)}}$, $\hat{\tilde{b}}_{w_{(i+1,j)}}$, $\hat{\tilde{b}}_{w_{(i-1,j)}}$, $\hat{\tilde{b}}_{w_{(i,j+1)}}$, $\hat{\tilde{b}}_{w_{(i,j-1)}}$ and assuming an arbitrary material distribution $\mu_w(u,v)$ on the facets we postulate:

$$\hat{\tilde{b}}_{w_{(k,l)}} = \int_{\Delta A_{w_{(k,l)}}} h_w(u,v) \cdot \mu_w(u,v)\, du\, dv, \quad (12)$$

with $(k,l) = \{(i,j),(i+1,j),(i-1,j),(i,j+1),(i,j-1)\}$. Evaluating (12) within an equidistant grid with homogeneous material distribution ($\mu_w(u,v) = \mu_w$) leads to the approximated flux through the inner facet $\Delta A_{w_{(i,j)}}$

$$\hat{\tilde{b}}_{w_{(i,j)}} = \mu_w \left(a_1 \cdot \Delta l_u \Delta l_v + a_4 \cdot \frac{\Delta {l_u}^3 \Delta l_v}{12}) + \right.$$
$$\left. + a_5 \cdot \frac{\Delta l_u \Delta {l_v}^3}{12} \right) + \mathcal{O}(\Delta l^6). \quad (13)$$

So the presented biquadratic approximation leads to a locally fourth order scheme for the normal field strength value $h_w(0,0) = a_1$ at the intersection point of dual edge $\Delta\tilde{l}_w$ and primary facet ΔA_w which is also the barycenter of this facet.

The resulting 5×5 linear system

$$\begin{pmatrix} \hat{\tilde{b}}_{w_{(i,j)}} \\ \hat{\tilde{b}}_{w_{(i+1,j)}} \\ \hat{\tilde{b}}_{w_{(i-1,j)}} \\ \hat{\tilde{b}}_{w_{(i,j+1)}} \\ \hat{\tilde{b}}_{w_{(i,j-1)}} \end{pmatrix} = \mathbf{M}^{(l)}_{\Delta A \mu} \cdot \begin{pmatrix} a_1 \\ a_2 \\ a_3 \\ a_4 \\ a_5 \end{pmatrix} \quad (14)$$

with the local surface integration matrix $\mathbf{M}^{(l)}_{\Delta A \mu}$ which can be inverted for each facet. Applying this conversion

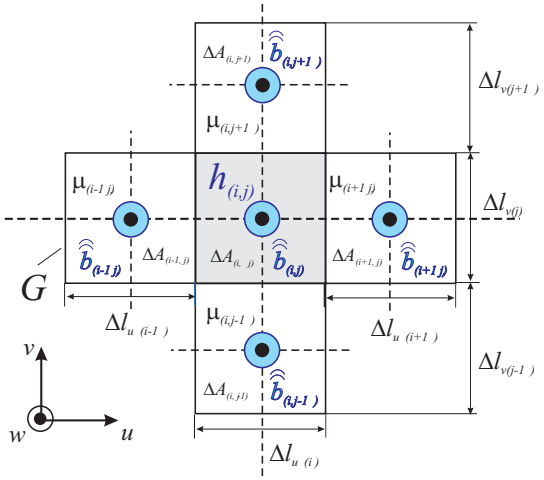

Fig. 4. Relation of the magnetic field strength value $h_{(i,j)}$ in w-direction located at the intersection point of dual edge $\Delta\tilde{l}_{(k)}$ and primary facet $\Delta A_{(i,j)}$ with the magnetic flux values $\hat{\tilde{b}}$ related to the facets of the primary grid.

scheme to all facets lead to the five-banded diagonal matrix

$$\mathbf{h} = \mathbf{M}_{(\Delta A \mu)^{-1}} \hat{\tilde{\mathbf{b}}} \quad (15)$$

containing information about metric and material distribution.

Fig.4 displays the magnetic fluxes $\hat{\tilde{b}}_w$, metric coefficients Δl_u, Δl_v and material values μ_w needed to compute $h_{w_{(i,j)}}$ located at the barycenter of the inner facet. Note that the material inside one primary cell can be distributed arbitrarily, only the material function $\mu_w(u,v)$ needs to be integratable over the considered facets.

For the standard discretization scheme (homogeneous material distribution within each cell as in most $FDTD$ implementations), as well as for advanced modeling approaches like triangular material fillings inside the cells, explicit formulas for the matrix coefficients can be derived.

C.2 Local Conversion of Field Strength to Flux Density

The scheme described above engenders a vector of normal magnetic field strength quantities localized at the intersection point of dual cell edges and normal facets. Obeying (5c) for surface charge free domains, the normal components of the magnetic flux density is continuous in inhomogeneous material distribution. So for calculating the magnetic voltage, the field strength component needs to be transformed locally into a flux density value (see Fig. 5) leading to the diagonal matrix

$$\mathbf{b} = \mathbf{M}_{\bar{\mu}} \mathbf{h}. \quad (16)$$

The described material relation does not involve metric coefficients, so it is free of any discretization error due to

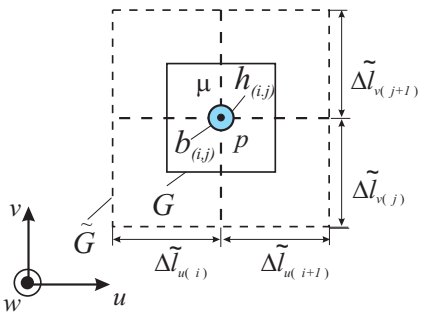

Fig. 5. Local transformation of tangential continuous magnetic field strength into normal continuous magnetic flux density at the intersection point p of normal facet and dual edge.

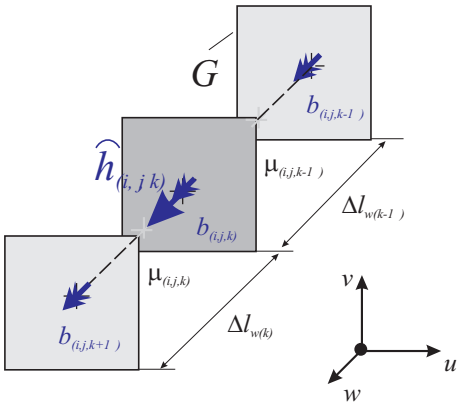

Fig. 6. Integration of normal continuous magnetic flux density function $b_w(w)$ along the dual edge to obtain the magnetic voltage $\widehat{h}_{w_{(k)}}$.

grid refinement, however the locally material smoothing inflicts an additional grid independent modeling error.

C.3 Integration of Voltage

Starting from magnetic flux values on facets, we derived in the normal direction to these facets a continuous flux density quantity. In order to integrate this flux density along the related edge to a voltage value, an interpolation function $b_w(w)$ is assumed coinciding at every intersection point of cell edge and corresponding dual facet with the former calculated normal flux density $h_{w_{(k)}} \cdot \mu_{w_{(k)}}$. For instance a localized quadratic approach for the flux density function in w-direction

$$b_w(w) = c_1 + c_2 \cdot w + c_3 \cdot w^2 \tag{17}$$

with the interpolation conditions

$$b_w(0) = h_{w_{(k)}} \cdot \mu_{w_{(k)}}, \tag{18a}$$

$$b_w(\Delta l_{w_{(k)}}) = h_{w_{(k+1)}} \cdot \mu_{w_{(k+1)}}, \tag{18b}$$

$$b_w(-\Delta l_{w_{(k-1)}}) = h_{w_{(k-1)}} \cdot \mu_{w_{(k-1)}} \tag{18c}$$

results in a 3×3 linear equation system for each dual edge. Having determined c_1, c_2 and c_3, the magnetic voltage can be integrated by use of the corresponding material distribution function $\mu_w(w)$ (see Fig. 6)

$$\widehat{h}_{w_{(k)}} = \int_{\Delta l_{w_{(k)}}} \frac{c_1 + c_2 \cdot w + c_3 \cdot w^2}{\mu_w(w)}\, dw. \tag{19}$$

Integrating (19) within an equidistant grid with homogeneous material distribution ($\mu_w(w) = \mu_w$) results in

$$\widehat{h}_{w_{(k)}} = \frac{1}{\mu_w}(c_1 \cdot \Delta l_w + c_3 \cdot \frac{\Delta l_w^3}{12}) + \mathcal{O}(\Delta l_w^5). \tag{20}$$

In the case of arbitrary grid spacing or inhomogeneous material the quadratic approach results in a local convergence rate of $\mathcal{O}(\Delta l^{4\cdots5})$.

Applied to all cell edges, the approach leads to a tridiagonal matrix converting magnetic flux density- into voltage quantities

$$\widehat{\mathbf{h}} = \mathbf{M}_{\Delta\bar{l}/\bar{\mu}}\mathbf{b}. \tag{21}$$

C.4 Higher Order Material Matrices for High Frequency Problems

Algorithms for high frequency problems, which will be described later in more detail, require numerical schemes for flux to voltage transformations. In the case of fourth order approximation and interpolation functions, denoted in (11) and (17), 15 flux values are required to calculate a single voltage value (see Fig. 7). The above described three step scheme results in modified material matrices

$$\widehat{\mathbf{e}} = \underbrace{\mathbf{M}_{\Delta l/\bar{\varepsilon}}\mathbf{M}_{\bar{\varepsilon}}\mathbf{M}_{(\Delta\bar{A}\bar{\varepsilon})^{-1}}}_{\mathbf{M}_{\varepsilon^{-1}}}\widehat{\widehat{\mathbf{d}}}, \tag{22a}$$

$$\widehat{\mathbf{h}} = \underbrace{\mathbf{M}_{\Delta\bar{l}/\bar{\mu}}\mathbf{M}_{\bar{\mu}}\mathbf{M}_{(\Delta A\mu)^{-1}}}_{\mathbf{M}_{\mu^{-1}}}\widehat{\widehat{\mathbf{b}}} \tag{22b}$$

and the local error of this flux-voltage transformation is $\mathcal{O}(\Delta l^{3\cdots5})$. In the case of an equidistant grid and homogeneous material distribution, the 15-banded material matrices (see Fig. 8) are positive semi definite. In terms of numerical efficiency it is advisable to store the surface derivation matrices $\mathbf{M}_{\bar{\mu}}\mathbf{M}_{(\Delta A\mu)^{-1}}$ and $\mathbf{M}_{\bar{\varepsilon}}\mathbf{M}_{(\Delta\bar{A}\varepsilon)^{-1}}$ and the line integration matrices $\mathbf{M}_{\Delta\bar{l}/\bar{\mu}}$ and $\mathbf{M}_{\Delta l/\bar{\varepsilon}}$ separately, which saves nearly 50% of CPU-time and memory.

D. Higher Order Voltage to Flux Transformation

The material matrices converting edge based (voltage) into surface based (flux) fields can be derived in

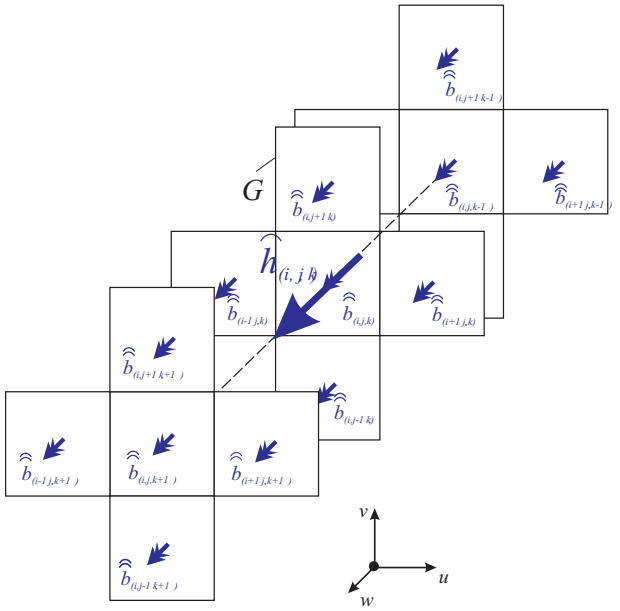

Fig. 7. Local transformation of magnetic flux $\widehat{\widehat{b}}$ into voltage quantities $\widehat{h}$ with the presented fourth order scheme. The calculation of one voltage value involves 15 flux values

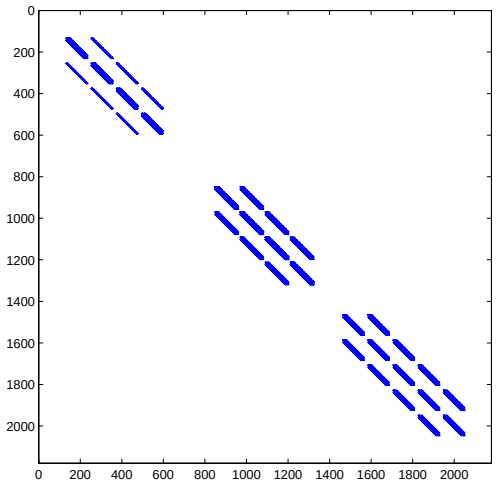

Fig. 8. Structure of the 15-banded $\mathbf{M}_{\varepsilon^{-1}}$ matrix of a cavity discretized with $10 \times 10 \times 5$ cells and PEC boundary.

a straightforward way. The basic steps are shortly denoted for the voltage-flux transformation of an electric voltage component in w-direction: The line integral of a higher order flux-density function $d_w(w)$ multiplied with the material weighting function $\varepsilon_w(w)$ approximates the voltages along the edges of a grid line. Converting the flux density d_w into a field strength quantity e_w at the intersection point of dual facet and corresponding edge enables the construction of a higher order field strength function $e_w(u, v)$ interpolating the derived field strength values. Once again the surface integration of the field strength function multiplied with the material weighting function $\varepsilon_w(u, v)$ enables the calculation of the flux $\widehat{\widetilde{d}}_w$ through the inner facet. For illustration purposes Fig. 9 displays the 15 relevant electric voltages for calculating one electric flux. Note that in contrast to the conventional scheme the voltage-flux matrix $\mathbf{M}_\varepsilon$ is the physical, but not the numerical inverse of the flux-voltage matrix $\mathbf{M}_{\varepsilon^{-1}}$, i.e. in general holds $\mathbf{M}_{\varepsilon^{-1}}^{-1} \neq \mathbf{M}_\varepsilon$.

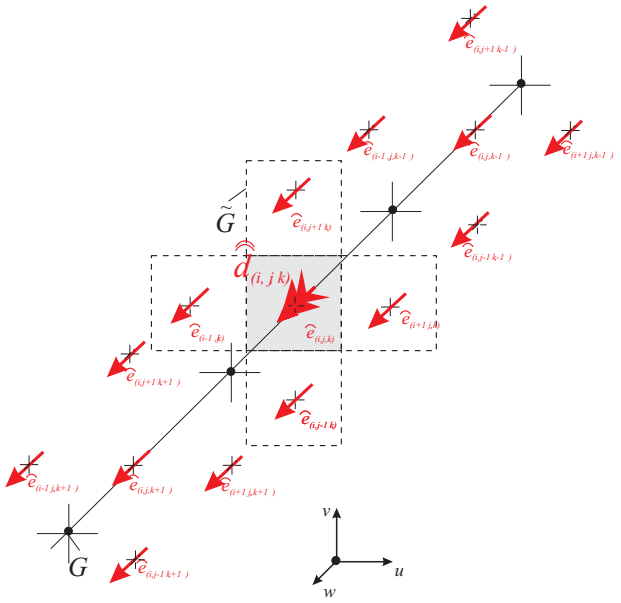

Fig. 9. Local transformation of electric voltage $\widehat{e}$ into electric flux values $\widehat{\widetilde{d}}$ with the presented fourth order scheme. The calculation of one flux value requires 15 voltage values.

E. Boundary Conditions

Since the enhanced flux-voltage and voltage-flux transformation leads to wideranging material matrices, the treatment of values at the boundary of the calculation area is more enhanced as in conventional *FIT*. PEC and PMC boundary properties are regarded as symmetry conditions for the normal and anti-symmetry conditions for the corresponding tangential field strength values at the boundary. Thus, the described algorithm can be applied straightforwardly for this kind of boundary conditions by choosing suitable even or odd higher order describing functions at the boundaries. The incorporation of open boundary conditions like Mur's ABC [17] or the popular PML-ABC [18] follows the conventional technique.

F. Numerical Efficiency

Applying the described fourth order technique, the simple diagonal material matrices of second order accuracy are replaced by 15-banded matrices, so the storage of the material matrix and the matrix-vector multiplication is drastically affected. Since the obtained matrices

are symmetric, just half of its components have to be stored, so the memory requirement for the fourth order scheme rises from N values (in the second order case) to $5N$ values. The CPU-time increases from N to $11N$ flops for one matrix-vector multiplication. Assuming that $\sqrt{N}$ points can be saved by maintaining the order of accuracy, the fourth order scheme is numerically cheaper than the conventional one if a high accuracy solution is required. Comparing the new approach with conventional higher order finite differences approach [7] (FD-4) reveals, that the memory consumption of both schemes is equal but computationally a single application of the new spatial operator costs 14 Flops (floating point operations) per field component in contrast to 11 Flops for the conventional FD-4 scheme thus leading to a 27% computational overhead.

IV. Frequency Domain Formulation

In the case of time harmonic problems, the electric curl-curl eigenvalue equation can be derived from (2a) and (2b)

$$\mathbf{M}_{\varepsilon^{-1}}\widetilde{\mathbf{C}}\mathbf{M}_{\mu^{-1}}\mathbf{C}\bar{\mathbf{e}} = \lambda\bar{\mathbf{e}} \tag{23}$$

with $\lambda = \omega^2$. The extraction of the lowest eigenfrequency of a cavity discretized with N cells requires to shift the nearly N zero eigenvalues caused by static modes to higher eigenvalues by imposing a grad div operation to the curl-curl equation. The Helmholtz eigenvalue problem [16]

$$(\mathbf{M}_{\varepsilon^{-1}}\widetilde{\mathbf{C}}\mathbf{M}_{\mu^{-1}}\mathbf{C} + \widetilde{\mathbf{S}}^T\mathbf{D}_s\widetilde{\mathbf{S}}\mathbf{M}_{\varepsilon^{-1}}^{-1})\bar{\mathbf{e}} = \lambda\bar{\mathbf{e}} \tag{24}$$

with the scaling matrix $\mathbf{D}_s$ ensures an appropriate shift of the static eigenvalues resulting in "ghost modes" which can easily be identified using FIT's consistency relation (3).

In the present approach, where $\mathbf{M}_{\varepsilon^{-1}}$ is a non-diagonal matrix and its numerical inverse $\mathbf{M}_{\varepsilon^{-1}}^{-1}$ can not be trivially computed, the modified formulation [20]

$$(\widetilde{\mathbf{C}}\mathbf{M}_{\mu^{-1}}\mathbf{C}\mathbf{M}_{\varepsilon^{-1}} + \widetilde{\mathbf{S}}^T\mathbf{D'}_s\widetilde{\mathbf{S}})\bar{\bar{\mathbf{d}}} = \lambda\bar{\bar{\mathbf{d}}} \tag{25}$$

for the electric flux with the modified shifting matrix $\mathbf{D'}_s$ can be used.

A. Grid Dispersion Relation

Assuming an infinite equidistant grid with the primary and dual cell edges Δ_u, Δ_v, Δ_w and a homogeneous material distribution with the values ε and μ, we consider the propagation of plane waves. Defining spatial phase factors $\underline{T}_u = e^{-jk_u\Delta_u}$, $\underline{T}_v = e^{-jk_v\Delta_v}$ and $\underline{T}_w = e^{-jk_w\Delta_w}$, the local version of the curl-curl matrix

$$\widetilde{\mathbf{C}}^{(l)}\mathbf{M}_{\mu^{-1}}^{(l)}\mathbf{C}^{(l)}\mathbf{M}_{\varepsilon^{-1}}^{(l)}\bar{\bar{\mathbf{d}}}^{(l)} = \lambda\bar{\bar{\mathbf{d}}}^{(l)} \tag{26}$$

can be constructed for the three components of one cell node resulting in a 3×3 eigenvalue problem with the three eigenvalues $\omega_i^2 = \lambda_i$. The three eigenvalues are $\omega_1 = 0$ (static modes) and the two-dimensional space of eigenvectors with the eigenvalues ω_2^2 and ω_3^2, reflecting the two possible polarization modes of the plane wave. This scheme leads to the formulation of a generalized grid dispersion relation with the eigenvalues

$$\begin{aligned}\omega_2^2 =& \mathbf{M}_{\varepsilon^{-1}}{}^{(l)}_{(3,3)}\mathbf{M}_{\mu^{-1}}{}^{(l)}_{(2,2)}\left(2\sin(\frac{k_u\Delta_u}{2})\right)^2 + \\ &+ \mathbf{M}_{\varepsilon^{-1}}{}^{(l)}_{(3,3)}\mathbf{M}_{\mu^{-1}}{}^{(l)}_{(1,1)}\left(2\sin(\frac{k_v\Delta_v}{2})\right)^2 + \\ &+ \mathbf{M}_{\varepsilon^{-1}}{}^{(l)}_{(1,1)}\mathbf{M}_{\mu^{-1}}{}^{(l)}_{(2,2)}\left(2\sin(\frac{k_w\Delta_w}{2})\right)^2, \end{aligned} \tag{27a}$$

$$\begin{aligned}\omega_3^2 =& \mathbf{M}_{\varepsilon^{-1}}{}^{(l)}_{(2,2)}\mathbf{M}_{\mu^{-1}}{}^{(l)}_{(3,3)}\left(2\sin(\frac{k_u\Delta_u}{2})\right)^2 + \\ &+ \mathbf{M}_{\varepsilon^{-1}}{}^{(l)}_{(1,1)}\mathbf{M}_{\mu^{-1}}{}^{(l)}_{(3,3)}\left(2\sin(\frac{k_v\Delta_v}{2})\right)^2 + \\ &+ \mathbf{M}_{\varepsilon^{-1}}{}^{(l)}_{(2,2)}\mathbf{M}_{\mu^{-1}}{}^{(l)}_{(1,1)}\left(2\sin(\frac{k_w\Delta_w}{2})\right)^2. \end{aligned} \tag{27b}$$

It is evident, that the transformation of surface based to edge based integral values has to be treated similarly for both quantities (i.e. $\mathbf{M}_{\varepsilon^{-1}}{}^{(l)}_{(2,2)}\mathbf{M}_{\mu^{-1}}{}^{(l)}_{(1,1)} = \mathbf{M}_{\varepsilon^{-1}}{}^{(l)}_{(1,1)}\mathbf{M}_{\mu^{-1}}{}^{(l)}_{(2,2)}$ etc.) to ensure a physical description of the plane wave propagation.

Necessary for physical consistency is the convergence of (27) to the analytic angular frequency

$$\omega^2 = \frac{1}{\mu\varepsilon}\left(k_u^2 + k_v^2 + k_w^2\right) \tag{28}$$

with $k_u = k\cos\phi\sin\theta$, $k_v = k\sin\phi\sin\theta$ and $k_w = k\cos\theta$, which can be revealed by means of Taylor expansion of the trigonometric expressions of (27) with $\lim_{\Delta\to 0}$ proofing the order of convergence.

Following the described scheme, a generalized local material matrix

$$\mathbf{M}^{(l)} = \varepsilon\mathbf{M}_{\varepsilon^{-1}}{}^{(l)} = \mu\mathbf{M}_{\mu^{-1}}{}^{(l)} \tag{29}$$

can be defined. Hereby conventional FIT uses coefficients

$$\mathbf{M}_{(1,1)}^{(l)} = \frac{\Delta_u}{\Delta_v\Delta_w}, \tag{30a}$$

$$\mathbf{M}_{(2,2)}^{(l)} = \frac{\Delta_v}{\Delta_u\Delta_w}, \tag{30b}$$

$$\mathbf{M}_{(3,3)}^{(l)} = \frac{\Delta_w}{\Delta_u\Delta_v} \tag{30c}$$

for the material matrix elements resulting in an order of $\mathcal{O}(\Delta^2)$ for (27). The proposed fourth order approach is

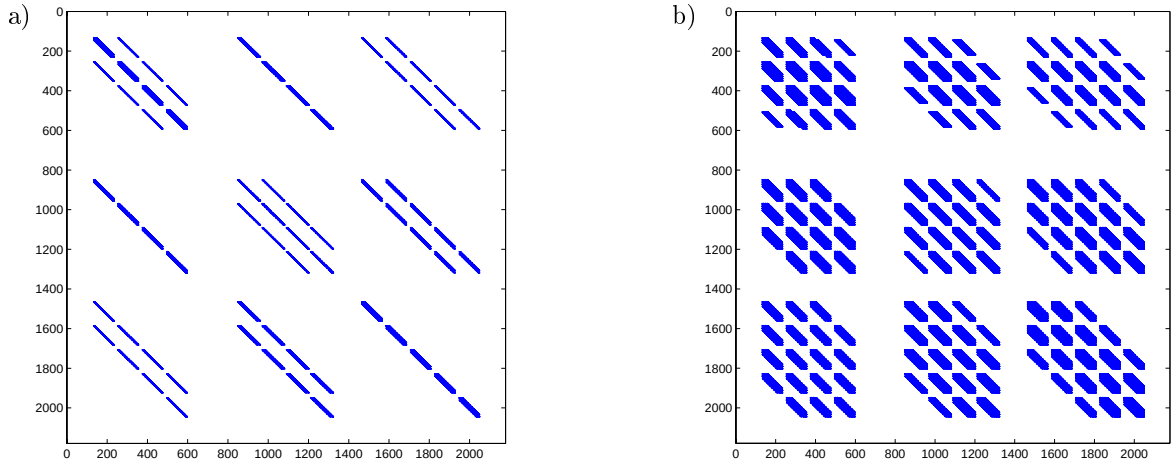

Fig. 10. Structure of the electric curl-curl matrix (23) with second order approach (a) and fourth order material matrices (b) of a cavity discretized with $10 \times 10 \times 5$ cells and PEC boundary condition.

described by the following matrix elements:

$$\mathbf{M}^{(l)}_{(1,1)} = \left[1 - \frac{1}{6}\sin^2\left(\frac{k_u\Delta_u}{2}\right)\right] \cdot \cdot \left[1 + \frac{1}{6}\left(\sin^2\left(\frac{k_v\Delta_v}{2}\right) + \sin^2\left(\frac{k_w\Delta_w}{2}\right)\right)\right] \frac{\Delta_u}{\Delta_v\Delta_w}, \tag{31a}$$

$$\mathbf{M}^{(l)}_{(2,2)} = \left[1 - \frac{1}{6}\sin^2\left(\frac{k_v\Delta_v}{2}\right)\right] \cdot \cdot \left[1 + \frac{1}{6}\left(\sin^2\left(\frac{k_u\Delta_u}{2}\right) + \sin^2\left(\frac{k_w\Delta_w}{2}\right)\right)\right] \frac{\Delta_v}{\Delta_u\Delta_w}, \tag{31b}$$

$$\mathbf{M}^{(l)}_{(3,3)} = \left[1 - \frac{1}{6}\sin^2\left(\frac{k_w\Delta_w}{2}\right)\right] \cdot \cdot \left[1 + \frac{1}{6}\left(\sin^2\left(\frac{k_u\Delta_u}{2}\right) + \sin^2\left(\frac{k_v\Delta_v}{2}\right)\right)\right] \frac{\Delta_w}{\Delta_u\Delta_v} \tag{31c}$$

and the Taylor expansion of (27) reveals an overall spatial convergence of $\mathcal{O}(\Delta^4)$. Figure 11 a) shows the enhanced dispersive character of the fourth order modeling in contrast to the second order approach of a time harmonic plane wave propagating transversely through an ideal equidistant homogeneous infinite grid. The direction dependent phase error at different spatial sampling rates is displayed in 11 b). The convergence rate of (27) using the generalized material matrix elements (30) respectively (31) and also of the conventional FD-4 scheme is displayed in a) and the direction dependent relative error of the FIT-4 and the FD-4 scheme in percent in b) of Fig. 12. The FD-4 scheme demonstrates a slightly lower dispersion error in every direction, the maximal relative error of the FIT-4 is approx 0.2% larger, which is quite negligible.

V. Spatial Stability

In order to obtain late-time stability of time-domain methods, the condition for the so-called spatial stability [19] of the curl-curl matrix (23) must hold: It states the need of real-valued positive eigenvalues of the curl-curl matrix, which is ensured in FIT by the rewritten form of (23)

$$(\mathbf{M}_\mu^{-1/2^T}\mathbf{C}\mathbf{M}_\varepsilon^{-1/2^T})^T \cdot (\mathbf{M}_\mu^{-1/2}\mathbf{C}\mathbf{M}_\varepsilon^{-1/2})\widehat{\mathbf{e}}' = \lambda\widehat{\mathbf{e}}' \tag{32}$$

with $\widehat{\mathbf{e}}' := \mathbf{M}_\varepsilon^{1/2}\widehat{\mathbf{e}}$. Necessary for this transformation are positive semidefinite material matrices $\mathbf{M}_{\varepsilon^{-1}}$ and $\mathbf{M}_{\mu^{-1}}$, which in conventional FIT is assured by diagonal matrices with non-negative entries.

In the case of a non-equidistant grid or inhomogeneous material distribution the fourth order method results in non-symmetric material matrices which can lead to complex-valued eigenvalues of (23) and an unstable update algorithm for time-domain simulation.

In order to reobtain a stable formulation, the symmetrization of the material matrices is enforced resulting in a local increase of discretization error. The underlying idea of the symmetrization process is an averaging of metric primitives and material values. Figure 13 displays metric coefficients needed for the calculation of two adjoined magnetic voltages $\widehat{h}_{w(1)}$ and $\widehat{h}_{w(2)}$, Fig.14 shows metric values, fluxes and material distribution for the calculation of the adjoint magnetic fluxes $\widehat{\widehat{b}}_{w(1,1)}$ and $\widehat{\widehat{b}}_{w(2,1)}$.

VI. Coupling of Fourth and Second Order Spatial Regions

The conventional FIT formulation offers a wide variety of enhanced spatial discretization techniques con-

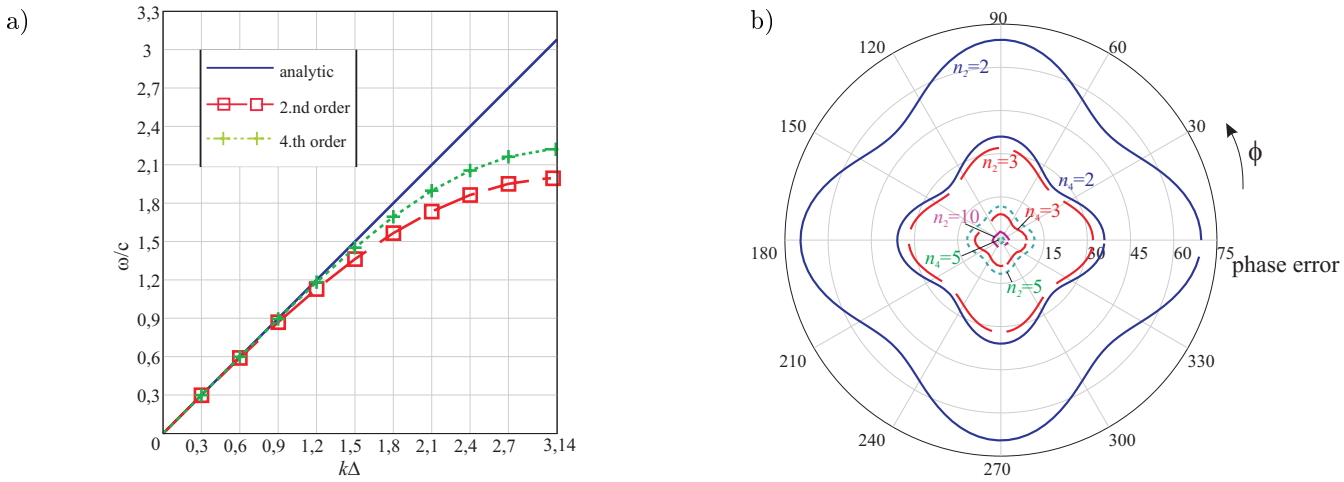

Fig. 11. The dispersion characteristic for a wave propagating in diagonally direction ($\theta = 54.7^o$, $\phi = 45^o$) is displayed in a). Fig. b) shows the phase error of k_{num} of the second (n_2) and fourth (n_4) material modeling at the sampling rates $n_{2/4} = \lambda/\Delta = 2, 3, 5$ and 10 in dependence of ϕ.

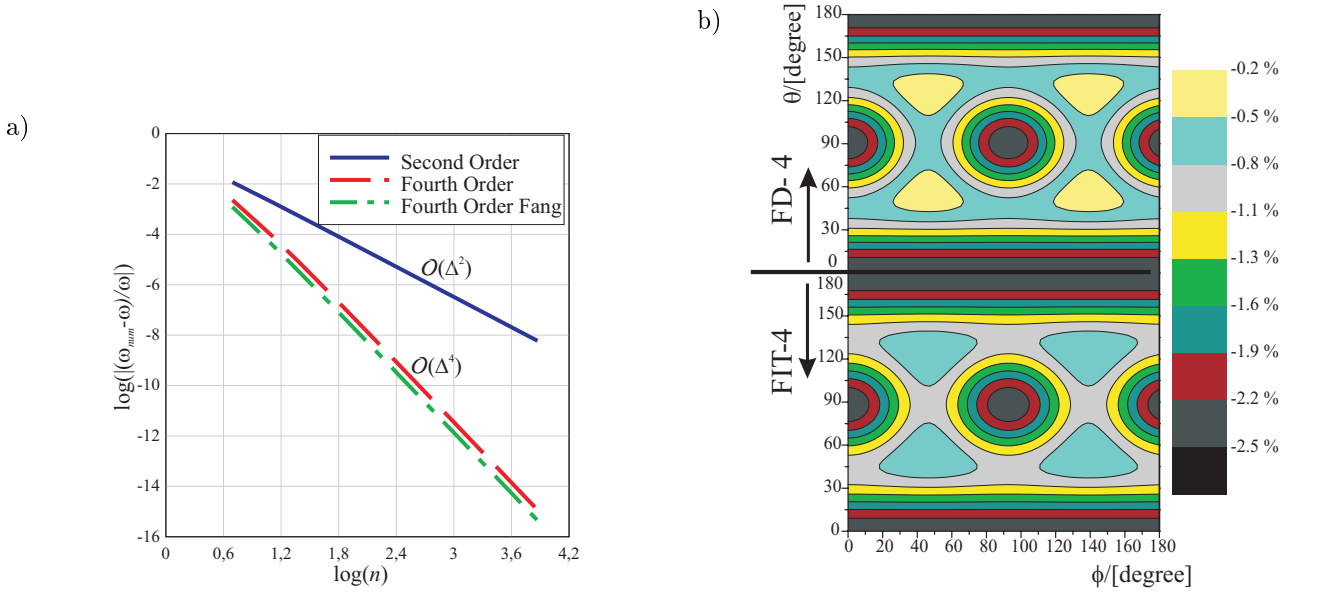

Fig. 12. Convergence of the spatial dispersion relation (27) to the exact solution in (28). Figure a) displays the relative error of the angular frequency ω_{num} of a plane wave traveling diagonally through the grid using second and fourth order material matrices and also the FD-4 operator in dependence of the number of grid steps per wavelength ($n = \lambda/\Delta$). Fig. b) displays the relative phase error in percent of the FIT-4 scheme (lower part) and of the FD-4 scheme (upper part) at a sampling rate of $n = \lambda/\Delta = 4$ as a function of the direction of wave propagation in the grid.

cerning the treatment of non-orthogonal grids [20], subgrids [21], dispersive [22], gyrotropic [23] or non-linear material modeling [24] and a lot of other specialized techniques.

As seen before, the fourth order spatial modeling is superior to the conventional scheme concerning dispersion, accuracy and convergence. Incorporating all these features in the fourth order technique would cause an enormous numerical effort and programming and lead to an unacceptable overhead in the computational process. To circumvent this problem, a low reflective, stable and easy to handle subdomain technique combining the advantages of second and fourth order material modeling has been developed. The underlying principle of the spatial stability, explained in section V, requires a symmetrical treatment of the components involved in the flux-voltage conversion process at the interface connecting the second- and the fourth order region, thus providing a symmetry relation for the involved quantities.

At the interface connecting the second and fourth order domains "mixed-order" functions describing the tangential and normal fields are used to ensure a symmetric

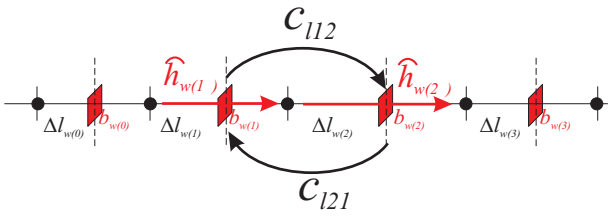

Fig. 13. Coupling coefficients for calculation of magnetic voltages from magnetic flux densities. Stability is guaranteed, if $c_{l12} = c_{l21}$.

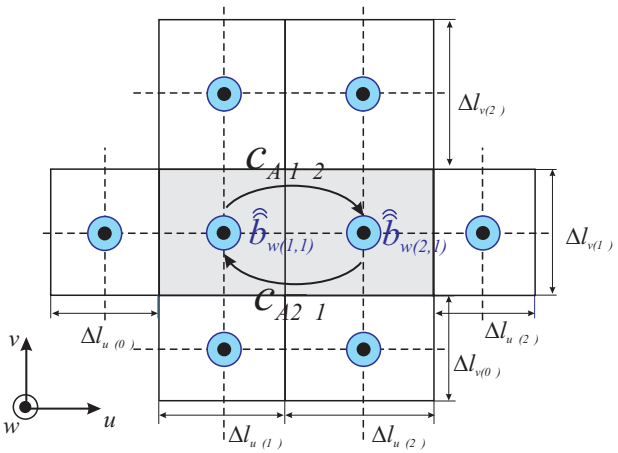

Fig. 14. Coupling coefficients for calculation of magnetic field strength values from magnetic fluxes. Stability is guaranteed, if $c_{A12} = c_{A21}$.

interaction of the involved quantities from both spatial domains. Figure 15 displays the structure of the $\mathbf{M}_{\varepsilon^{-1}}$ matrix of a cavity modeled with the hybrid scheme.

VII. Example

The presented method of fourth order spatial discretization is applied to a simple three dimensional rectangular cavity with the dimensions 1m×1m×0.5m and PEC boundary conditions. The analytical resonance frequency of the configuration's lowest mode is $f_{TM_{110}} = f_{TE_{110}} = 212.13$ MHz. The size of the cell edges is varied from $\lambda/3$ down to $\lambda/17$.

A. Spatial Convergence

To study the convergence behavior of the fourth order material matrices due to grid refinement, the resonance frequency is calculated in the frequency domain using (24) respectively (25) with refinement of the cell edges. In the equidistant case a convergence rate of $\mathcal{O}(\Delta^{2.04})$ for the conventional method and - as expected - of $\mathcal{O}(\Delta^{4.55})$ in the fourth order case can be observed. The convergence rates of the eigenfrequencies are displayed in Fig. 16 a). In the non-equidistant case, whereby the spatial step is reduced from one edge to the next by 5%,

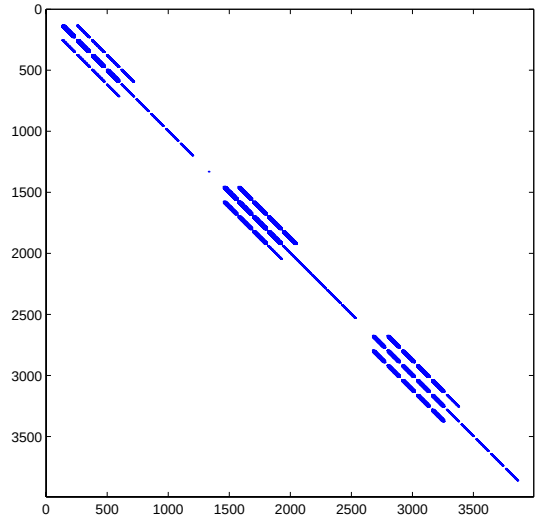

Fig. 15. Structure of a mixed second-fourth order $\mathbf{M}_{\varepsilon^{-1}}$ matrix of a cavity discretized with $10 \times 10 \times 10$ cells and PEC boundary. Half of the calculation domain is discretized with the fourth order approach, the other one with conventional second order scheme.

the frequency domain analysis displayed in Fig. 17 a) demonstrates a convergence rate of $\mathcal{O}(\Delta^{1.87})$ for the second order and $\mathcal{O}(\Delta^{4.18})$ for the fourth order formulation.

B. Time Domain Convergence

Higher order time domain formulations are called (N, X)-schemes, N describing the order of temporal integration and X the order of the spatial operators. Full fourth order explicit time domain schemes ((4,4) schemes) require a fourth order spatial scheme as well as a fourth order time integration method [25]. For time-domain analysis of the convergence behavior, we impose a Gaussian-formed pulse with 200MHz center frequency and 80MHz bandwidth stimulating the TM_{110} mode. The stimulating dipole is located at the center of the computational domain. The time step size is chosen as $\Delta t = 0.75 \cdot \Delta t_{courant}$, and the resonance frequency is extracted by means of Discrete Frequency Transformation (DFT).

The numerically computed overall convergence order in the case of an equidistant grid is $\mathcal{O}(\Delta^{2.7})$ for the (2,2) Leap-Frog scheme. The fourth order scheme with a fourth order version of the Leap-Frog update equations ((4,4)-scheme) exhibits an unexpected high convergence rate of $\mathcal{O}(\Delta^{7.9})$. A hybrid (4,4-2) Leap-Frog formulation [25], with a reduced computational effort per time step uses fourth and second order material matrices and demonstrates an overall convergence of $\mathcal{O}(\Delta^{4.8})$ (see Fig. 16 b). The same analysis with a non-equidistant grid (Fig. 17 b) demonstrates a convergence rate of $\mathcal{O}(\Delta^{2.28})$ for the (2,2) and $\mathcal{O}(\Delta^{4.85})$ for the (4,4) scheme.

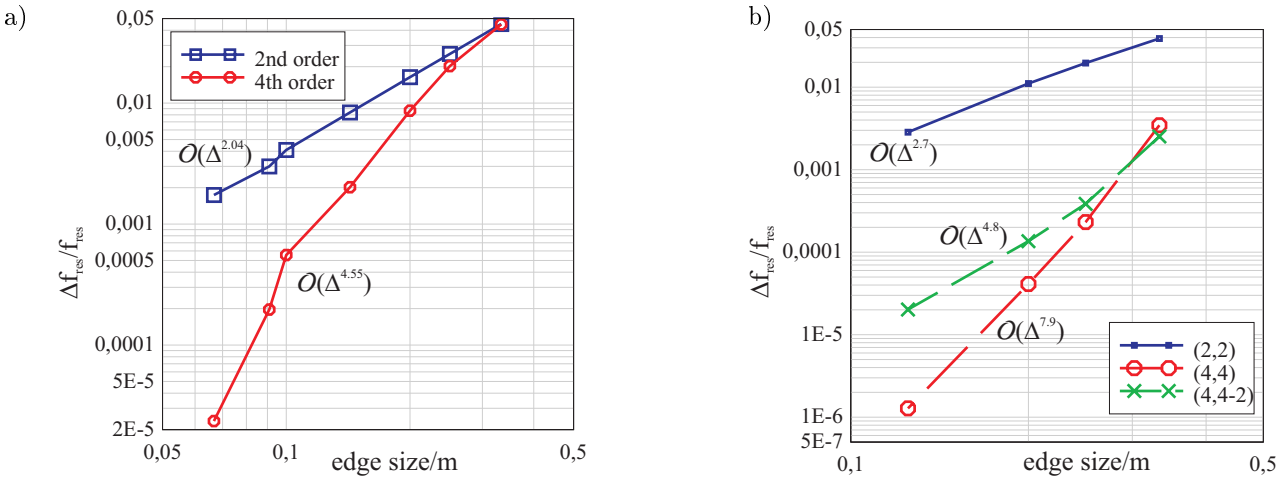

Fig. 16. Frequency-domain (a) and time-domain (b) convergence of the lowest eigenmode of the rectangular cavity. The frequency domain analysis was performed by calculating the eigenvalues of the curl-curl matrix (25). The time domain analysis shows the convergence rate of the (2,2), (4,4) and a hybrid (4,4-2) $FITD$ scheme.

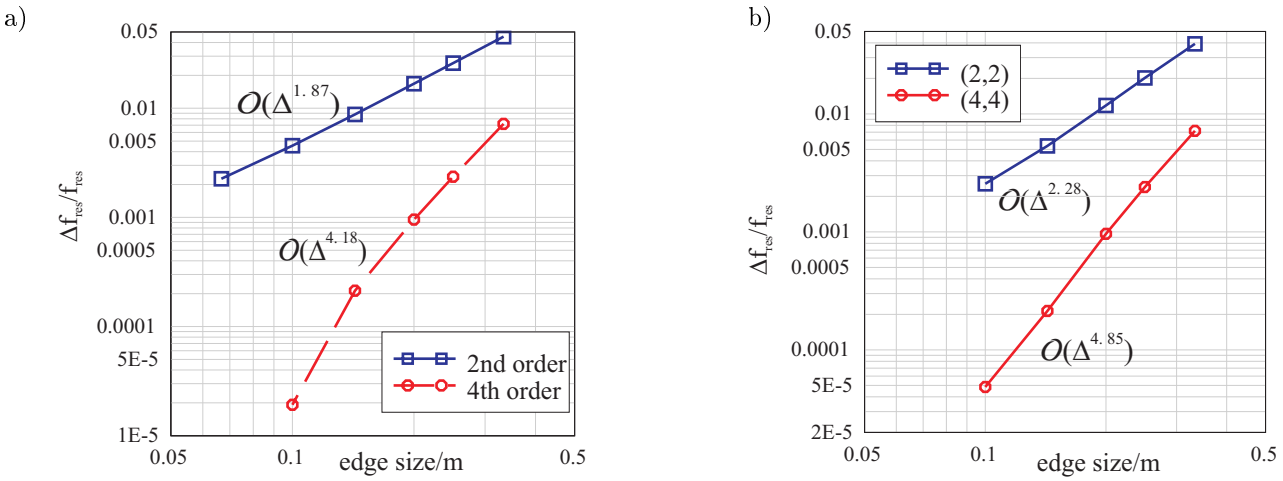

Fig. 17. Frequency Domain (a) and Time Domain (b) convergence of the lowest eigenmode of the rectangular cavity discretized by a non-uniform grid where the edge lengths are defined by $\Delta_{i+1} = 0.95\Delta_i$.

The improvement of the time-domain convergence rate of the (2,2) scheme in comparison to the second order frequency-domain modeling results from a partial compensation of time-integration and spatial discretization error having different signs. A similar effect is assumed to be responsible for the extreme convergence rate of the (4,4) scheme.

VIII. Conclusion

In this paper a general extension of the FIT-algorithm towards higher order spatial resolution is proposed.

FIT formulations for all systems of coupled differential equations following these properties can be extended to the presented higher order technique, exemplarily the Maxwellian system is discussed.

The new scheme is based on modified material matrices for the transformation of grid fluxes into grid voltages and vice versa, which is the only modeling step in FIT where approximations are introduced. Within these matrices, higher order piece-wise defined polynomials are applied for the interpolation of the field quantities, taking care of all physical continuity relations. A generalized grid-dispersion equation is derived and analyzed to demonstrate the convergence of the fourth order approach. The stability of the new scheme is ensured by the symmetrization of the resulting material matrices. A coupling technique for the interface of second order and fourth order domains is discussed.

In comparison to existing finite difference techniques, the presented scheme demonstrates the same dispersion characteristics and nearly the same computational cost, but all the consistency and conservation properties of

FIT are remained, which is not always guaranteed by conventional *FD* schemes.

An analysis of the lowest eigenmode of a simple configuration in frequency and time domain using a fourth order Leap-Frog scheme verifies the superior convergence rate of the fourth order formulation. The new approach represents a vital enhancement for the applicability of the *FIT* method to electrically larger problems and can also be used in existing codes for error estimation purposes.

References

[1] T. Weiland *"A Discretization Method for the Solution of Maxwell's Equations for Six-Component Fields"*, Electronics and Communication (AEÜ), Vol. 31, p. 116-120, 1977

[2] J. E. Castillo, J. M. Hyman, M. Shashkov, S. Steinberg *"The Sensitivity and Accuracy of Fourth Order Finite-Difference Schemes on Nonuniform Grids in One Dimension"*, Computers Math. Applic., Vol. 30, No. 8., pp. 41-55, 1995

[3] M. F. Hadi *"A Modified FDTD (2,4) Scheme for Modeling Electrically Large Structures with High Phase Accuracy"*, Ph.D. Dissertation, ECEN Dept., University of Colorado, Boulder, CO, 1996

[4] N. V. Kantartzis, T. D. Tsiboukis *"A Generalized Methodology based on Higher-Order Conventional and Non-Standard FDTD Concepts for the Systematic Development of Enhanced Dispersionless Wide-Angle Absorbing Perfectly Matched Layers "*, International Journal of Numerical Modeling, Vol. 13, No. 5, pp. 417-440, 2000

[5] I. Harari, E. Turkel *"Accurate Finite Difference Methods for Time-Harmonic Wave Propagation"*, Journal of Computational Physics, No. 119, pp. 253-270, 1995

[6] N. Homsup *"A Comparision between a Spline-Based Method and a High-Order FDTD Scheme for the Maxwell Equations"*, Proc. of Computational Electromagnetics and its Applications (ICCEA), Bejing, China, Nov. 1.-4., pp. 56-59, 1999

[7] J. Fang *"Time Domain Finite Difference Computation for Maxwell's Equations"*, PhD. dissertation, EECS Dept.,Univ. California, Berkeley, CA, 1989

[8] J. L. Young, D. Gaitonde, J. J. S. Shang *"Toward the Construction of a Fourth-Order Difference Scheme for Transient EM Wave Simulation: Staggered Grid Apporach"*, IEEE Transactions on Antennas and Propagation, Vol. 45, No. 9, pp. 1573-1581, 1997

[9] J. L. Young *"A Higher Order FDTD Method for EM Propagation in a Collisionless Cold Plasma"*, IEEE Transactions on Antennas and Propagation, Vol. 44, No. 9, pp. 1283-1289, 1996

[10] E. Turkel, A. Yefet *"Fourth Order Accurate Compact Implicit Method for the Maxwell Equation"*, http://www.math.tau.ac.il/∼turkel/

[11] K. P. Hwang, A. C. Cangellaris *"Numerical Boundary Conditions at Material Interfaces for High-Order FDTD Schemes"*, Proceedings of 17'th ACES Conference, Monterey, USA, pp 8-15, 2001

[12] Z. Xie, B. Zhang, C. H. Chan *"A Fourth-Order Accurate Staggered FD-TD scheme for the Maxwell Equations"*, Proc. of IEEE Antennas and Propagation Society (AP-S), Salt Lake City, USA, pp. 1518-1521, July. 16.-21. 2000

[13] M. Krumpholz, L. P. B. Katehi *"MRTD: New Time-Domain Schemes Based on Multiresolution Analysis"*, IEEE Transactions on Microwave Theory and Techniques, Vol. 44, No. 4., pp. 555-571, 1996

[14] M. Clemens, R. Schuhmann, T. Weiland *"Algebraic Properties and Conservation Laws in the Discrete Electromagnetism "*, Frequenz, No. 53, pp. 219-225, 1999

[15] T. Weiland *"Time Domain Electromagnetic Field Computation With Finite Difference Methods"*, International Journal of Numerical Modeling, Vol. 9, pp. 295-319, 1996

[16] T. Weiland *"On the Unique Numerical Solution of Maxwellian Eigenvalue Problems in three Dimensions"*, Particle Accelerators, Vol. 17, pp. 227-242, 1985

[17] G. Mur *"Absorbing Boundary Conditions for the Finite-Difference Approximation of the Time-Domain Electromagnetic Field Equations"*, IEEE Trans. Electromagn. Compat., Vol. EMC-23, pp 377-382, Nov. 1981

[18] J. R. Berenger *"A Perfectly Matched Layer for the Absorption of Electromagnetic Waves"*, J. Computat. Phys., Vol. 114, pp. 185-200, Oct. 1994

[19] P. Thoma, T. Weiland *"Numerical Stability of Finite Difference Time Domain Methods"*, IEEE Transactions on Magnetics, Vol. 34, No. 5, September 1998

[20] R. Schuhmann, T. Weiland *"FDTD on Nonorthogonal Grids with Triangular Fillings"*, IEEE Transactions on Magnetics, Vol. 35, No. 3, pp. 1470-1473, May 1999

[21] P. Thoma, T. Weiland *"A Consistent Subgridding Scheme for the Finite Difference Time Domain Method"*, International Journal of Numerical Modelling, Vol. 9, pp. 359-374, 1996

[22] S. Gutschling, H. Krüger, T. Weiland *"Time Domain Simulation of Dispersive Media with the Finite Integration Technique"*, International Journal of Numerical Modelling, Vol. 13, No. 4, pp. 329-348, 2000

[23] T. Weiland, H. Krüger, H. Spachmann *"FIT-Formulation for Gyrotropic Media"*, Internat. Conference on Electromagnetics in Advanced Applications (ICEAA '99), Sept. 13-17, Torino, Italy, pp. 737-740, 1999

[24] H. Spachmann, S. Gutschling, H. Krüger, T. Weiland *"FIT-Formulation for Nonlinear Dispersive Media"*, International Journal of Numerical Modelling, Special Issue, Vol. 12, No. 1/2, pp. 81-92, 1999

[25] H. Spachmann, R. Schuhmann, T. Weiland *"Convergence, Stability and Dispersion Analysis of Higher Order Leap-Frog Schemes for Maxwell's Equations"*, Proceedings of 17'th ACES Conference, Monterey, USA, pp 655-662, 2001